

Alfvén waves in dusty plasmas with plasma particles described by anisotropic kappa distributions

R. A. Galvão, L. F. Ziebell, R. Gaelzer, and M. C. de Juli

Citation: *Phys. Plasmas* **19**, 123705 (2012); doi: 10.1063/1.4772771

View online: <http://dx.doi.org/10.1063/1.4772771>

View Table of Contents: <http://pop.aip.org/resource/1/PHPAEN/v19/i12>

Published by the [American Institute of Physics](#).

Related Articles

Simulation of neoclassical transport with the continuum gyrokinetic code COGENT

Phys. Plasmas **20**, 012513 (2013)

Nonlinear dynamics of beta-induced Alfvén eigenmode in tokamak

Phys. Plasmas **20**, 012510 (2013)

Gyrokinetic simulation of global and local Alfvén eigenmodes driven by energetic particles in a DIII-D discharge

Phys. Plasmas **20**, 012508 (2013)

Investigation of an ion-ion hybrid Alfvén wave resonator

Phys. Plasmas **20**, 012111 (2013)

Gyrokinetic simulations of reverse shear Alfvén eigenmodes in DIII-D plasmas

Phys. Plasmas **20**, 012109 (2013)

Additional information on Phys. Plasmas

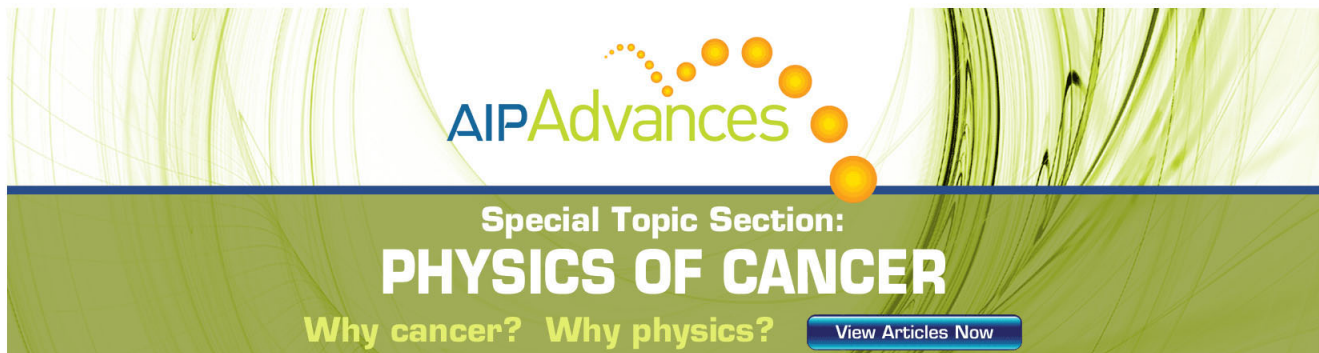
Journal Homepage: <http://pop.aip.org/>

Journal Information: http://pop.aip.org/about/about_the_journal

Top downloads: http://pop.aip.org/features/most_downloaded

Information for Authors: <http://pop.aip.org/authors>

ADVERTISEMENT



AIP Advances

Special Topic Section:
PHYSICS OF CANCER

Why cancer? Why physics? [View Articles Now](#)

Alfvén waves in dusty plasmas with plasma particles described by anisotropic kappa distributions

R. A. Galvão,¹ L. F. Ziebell,^{1,a)} R. Gaelzer,² and M. C. de Juli³

¹Instituto de Física, Universidade Federal do Rio Grande do Sul, Caixa Postal 15051, CEP: 91501-970, Porto Alegre, Rio Grande do Sul, Brazil

²Instituto de Física e Matemática, Universidade Federal de Pelotas, Caixa Postal 354—Campus UFPel, CEP: 96010-900 Pelotas, Rio Grande do Sul, Brazil

³Centro de Rádio-Astronomia e Astrofísica Mackenzie—CRAAM, Universidade Presbiteriana Mackenzie, Rua da Consolação 896, CEP: 01302-907 São Paulo, São Paulo, Brazil

(Received 14 September 2012; accepted 30 November 2012; published online 27 December 2012)

We utilize a kinetic description to study the dispersion relation of Alfvén waves propagating parallelly to the ambient magnetic field in a dusty plasma, taking into account the fluctuation of the charge of the dust particles, which is due to inelastic collisions with electrons and ions. We consider a plasma in which the velocity distribution functions of the plasma particles are modelled as anisotropic kappa distributions, study the dispersion relation for several combinations of the parameters κ_{\parallel} and κ_{\perp} , and emphasize the effect of the anisotropy of the distributions on the mode coupling which occurs in a dusty plasma, between waves in the branch of circularly polarized waves and waves in the whistler branch. © 2012 American Institute of Physics. [<http://dx.doi.org/10.1063/1.4772771>]

I. INTRODUCTION

The solar wind is an outflow of plasma coming out of the solar corona and traveling through the heliosphere. It is composed mostly by electrons and protons, with a much smaller population of alpha particles and heavier ions, containing also a population of dust particles which in terms of number density is much less expressive than the population of electrons and ions.^{1,2} Similar outflows must also occur around other stars, what makes the solar wind a representative of a more general class of phenomena, which can receive the general denomination of stellar winds.

Dust particles have been observed in the solar wind, both by remote sensing and by direct observation by spacecrafts, covering a range of distances starting from the inner solar system and extending outside up to a few AU's (astronomical units).³⁻⁶ The observations have been made inside a region within angular distance of 30° from the ecliptic plane. In the region covered by the observations, the typical dust particles have been seen to be of nanometrical size, with mass $\geq 10^{-20}$ g. Despite the small value of the number density, it is estimated that the mass of dust per unit volume in the interplanetary space can be about one order of magnitude larger than the density of mass associated to the solar wind particles.⁷⁻⁹

Of particular interest for the present work are the observations which have shown that the velocity distribution functions of the main components of the solar wind feature marked non-thermal characteristics. For instance, the proton distribution was measured by the IMP 6, HELIOS, Wind and Ulysses spacecraft within the radial interval from 0.3 to 2.5

AU, displaying a significant temperature anisotropy, with the perpendicular temperature ($T_{\perp p}$) (relative to the local interplanetary magnetic field) larger than the parallel temperature ($T_{\parallel p}$) at 0.3 AU, but with $T_{\parallel p} > T_{\perp p}$ for radial distances greater than 1 AU.^{1,10-12} The free energy available in the non-Maxwellian distribution can lead to plasma instabilities related to the protons that are, for a bi-Maxwellian distribution, the proton cyclotron, mirror and parallel and oblique firehose instabilities. However, comparisons made between the observed wave levels and the linear theory of plasma instabilities have shown that the observations are not adequately described by the theoretical results obtained employing a simple bi-Maxwellian distribution.^{1,13}

The distribution function for electrons has also been observed to possess significant non-thermal characteristics. According to observations, these distribution functions are typically composed by a dense thermal core with low energy and two tenuous but hot superthermal populations, the *halo*, which is present at all pitch angles, and the *strahl*, which is a highly anisotropic population moving along field lines in the anti-sunward direction.¹⁴⁻²³ Due to the observed non-thermal characteristics, the electron distribution has been modeled in recent years by Lorentzian or kappa distributions,²⁴⁻²⁷ and the same type of distributions has been proposed for modeling the proton distribution functions.²⁸ The kappa distribution can be characterized by the κ index, with the Maxwellian distribution being the asymptotic limit for $\kappa \rightarrow \infty$. Fitting of data obtained by spacecraft in the range 0.3–4 AU have shown that in that region of the solar wind, the κ index drops monotonically with radial distance for both the halo and *strahl* components, with $\kappa \simeq 2$ for $R_S \simeq 4$ AU and $10 \lesssim \kappa \lesssim 16$ for $R_S \simeq 0.3$ AU.^{26,27} Over the whole distance range, the electron distribution functions are noticeably different from the Maxwellian.

^{a)}Electronic address: ziebell@if.ufrgs.br.

The observation that particle distributions in the space environment are frequently non-thermal is backed up by many theoretical analysis. In fact, several mechanisms have been proposed as responsible for the creation of the observed non-thermal features, including the so-called exospheric theory of the solar wind electrons,^{18,21} the broadening of the *strahl* by pitch-angle and diffusion due to wave-particle interactions,^{26,27} and non-thermal states, which satisfy conditions of turbulent equilibrium between waves and particles.²⁹ Since the space plasmas are frequently collisionless, they are not easily thermalized to the Maxwellian state and preserve the non-thermal features, which are generated by other physical mechanisms. The non-thermal features associated to κ distributions can lead to significant effects on wave dispersion relations, which have motivated many recent investigations, as in Refs. 30–32.

It is known that the presence of dust may affect considerably the dynamics of waves in the interplanetary plasma. Also in laboratory experiments, it has been shown that non-equilibrium features in the electron distribution function may strongly affect the distribution of charge of dusty grains.³³ In particular, in the case of Alfvén waves in spacelike conditions, for instance, we have already discussed the modification of damping due to collisional charging of dust particles,³⁴ and the occurrence of mode coupling between the whistler and the ion cyclotron branch.^{35,36} These analysis have been made for the case of Maxwellian distributions for ions and electrons. More recently, we have explored the combined effect of the non-Maxwellian features of kappa distributions and the presence of dust, combination which originate considerable modifications in the dispersion relation for Alfvén waves.³⁷

In the present work, we develop further the investigation by exploring the anisotropic features which have been observed in the solar wind, by considering a magnetized dusty plasma in which the electrons and ions are described by anisotropic kappa distributions. In Sec. II, we introduce the dusty plasma model and the velocity distribution functions for electrons and ions, and also the frequencies of inelastic collisions between dust particles and plasma particles, as well as the equilibrium electric charge of the dust particles. In Sec. III, we present the dispersion relation for parallel-propagating Alfvén waves, and in Sec. IV, we present and discuss results obtained by numerical solution of the dispersion relation. Final remarks and a discussion on future perspectives appear in Sec. V.

II. DUSTY PLASMA MODEL

We consider a magnetized dusty plasma in which the magnetic field is along the z direction, $\mathbf{B}_0 = B_0 \mathbf{e}_z$, with a dust population composed by groups of particles, which are assumed to be spherical with different radius a_j and charge q_j , where $j = 1, \dots, n$, which is acquired by capturing plasma particles by inelastic collisions. We assume that in the average, the electrostatic energy associated to the interaction between dust particles is much smaller than their kinetic energy, so that the analysis is restricted to the case of weakly coupled dusty magneto-plasmas. We also assume that the dust particles can be considered immobile, which

means that the wave angular frequency ω is much larger than the dust plasma frequency ω_{pd} and the dust cyclotron frequency Ω_d ($\omega \gg \omega_{pd} \gg |\Omega_d|$). As a consequence, the formulation excludes the wave modes originated from the dust dynamics.

The distribution of plasma particles of species β satisfies a Vlasov meta equilibrium with the addition of a term associated to inelastic collisions with dust particles, which can, therefore, capture plasma particles. The formalism includes the interaction between the plasma particles and dust particles of all populations.

More explicitly, the f_β distributions satisfies the following equation:

$$\begin{aligned} \frac{\partial f_\beta}{\partial t} + \frac{\mathbf{p}}{m_\beta} \cdot \nabla f_\beta + q_\beta \left[\mathbf{E} + \frac{\mathbf{p}}{m_\beta c} \times \mathbf{B} \right] \cdot \nabla_{\mathbf{p}} f_\beta \\ = - \int dq \frac{p}{m_\beta} \sum_j \sigma_\beta^j (f_{d0}^j f_\beta - f_{d0}^j f_{\beta 0}), \end{aligned} \quad (1)$$

where f_{d0}^j and $f_{\beta 0}$ represent, respectively, the equilibrium distribution function of dust particles of species j and of plasma particles of species β , and σ_β^j is the cross section for charging of dust particles of radius a_j by inelastic collisions with particles of species β , given by³⁸

$$\sigma_\beta^j(p, q) = \pi a_j^2 \left(1 - \frac{2qq_\beta m_\beta}{a_j p^2} \right) H \left(1 - \frac{2qq_\beta m_\beta}{a_j p^2} \right). \quad (2)$$

The distribution function for the dust particles of population j , $f_d^j \equiv f_d^j(\mathbf{r}, q, t)$, satisfies the following equation:

$$\frac{\partial f_d^j}{\partial t} + \frac{\partial}{\partial q} [I^j(\mathbf{r}, q, t) f_d^j] = 0, \quad (3)$$

where

$$I^j(\mathbf{r}, q, t) = \sum_\beta \int d^3 p q_\beta \sigma_\beta^j(p, q) \frac{p}{m_\beta} f_\beta(\mathbf{r}, \mathbf{p}, t)$$

is the current of electrons and ions, which charge the dust particles.³⁹

Considering small amplitude oscillations, the perturbed distribution function satisfies the following equation:

$$\begin{aligned} \frac{\partial f_{\beta 1}}{\partial t} + \frac{\mathbf{p}}{m_\beta} \cdot \nabla f_{\beta 1} + q_\beta \left(\frac{\mathbf{p}}{m_\beta c} \times \mathbf{B}_0 \right) \cdot \nabla_{\mathbf{p}} f_{\beta 1} \\ + \left(\sum_j \nu_{\beta d}^j(p) \right) f_{\beta 1} = - \left(\sum_j \nu_{\beta d}^j(\mathbf{r}, p, t) \right) f_{\beta 0} \\ - q_\beta \left[\mathbf{E}_1 + \frac{\mathbf{p}}{m_\beta c} \times \mathbf{B}_1 \right] \cdot \nabla_{\mathbf{p}} f_{\beta 0}, \end{aligned} \quad (4)$$

where

$$\nu_{\beta d}^j(p) \equiv \int_{-\infty}^0 \sigma_\beta^j(p, q) \frac{p}{m_\beta} f_{d0}^j(q) dq,$$

$$\nu_{\beta d}^{j1}(\mathbf{r}, p, t) \equiv \int_{-\infty}^0 \sigma_{\beta}^j(p, q) \frac{p}{m_{\beta}} f_{d1}^j(\mathbf{r}, q, t) dq.$$

Using Fourier-Laplace transform in the system of equations, it is readily shown that the perturbed distribution function for species β can be written as

$$\hat{f}_{\beta}(\mathbf{p}) = \hat{f}_{\beta}^C + \hat{f}_{\beta}^N, \tag{5}$$

where

$$\begin{aligned} \hat{f}_{\beta}^C &= -q_{\beta} \int_{-\infty}^0 d\tau e^{i\{\mathbf{k}\cdot\mathbf{R} - [\omega + i(\sum_j \nu_{\beta d}^{j0}(p))]\tau\}} \\ &\quad \times \left(\hat{\mathbf{E}} + \frac{\mathbf{p}'}{m_{\beta}c} \times \hat{\mathbf{B}} \right) \cdot \nabla_{\mathbf{p}'} f_{\beta 0}(p_{\perp}, p_{\parallel}), \\ \hat{f}_{\beta}^N &= - \int_{-\infty}^0 d\tau e^{i\{\mathbf{k}\cdot\mathbf{R} - [\omega + i(\sum_j \nu_{\beta d}^{j0}(p))]\tau\}} \\ &\quad \times \left(\sum_j \hat{\nu}_{\beta d}^j(\mathbf{k}, p, \omega) \right) f_{\beta 0}. \end{aligned}$$

These expressions are similar to those appearing in Ref. 40, except for the fact that in the present paper, there is a summation over the inelastic equilibrium collision frequencies $\nu_{\beta d}^{j0}(p)$ in the argument of the exponential functions, instead of a single collision frequency, as well as a summation over the Fourier-Laplace transforms of the perturbed collision frequency $\nu_{\beta d}^{j1}$ in the integrand of \hat{f}_{β}^N , instead of a single value.

It is noticed that \hat{f}_{β}^C has the same formal structure as the perturbed distribution obtained in the evaluation of the dielectric tensor of a conventional homogeneous magnetized plasma, with $\omega + i\sum_j \nu_{\beta d}^{j0}(p)$ instead of ω in the argument of the exponential function, and originates a contribution to the dielectric tensor, which can be called the ‘‘conventional’’ contribution, denoted as ϵ_{ij}^C .^{40,41} The quantity identified as \hat{f}_{β}^N , in addition to a similar contribution to the argument of the exponential function, features an integrand which is proportional to $\sum_j \hat{\nu}_{\beta d}^j$ and which vanishes in the case of dustless plasma. It constitutes a contribution to the dielectric tensor which is exclusive to dusty plasmas, and which can therefore be called the ‘‘new’’ contribution, denoted as ϵ_{ij}^N .^{40,41} The components of the dielectric tensor therefore can be written as a summation of these two contributions⁴⁰⁻⁴²

$$\epsilon_{ij} = \epsilon_{ij}^C + \epsilon_{ij}^N. \tag{6}$$

The development of the expression proceeds as in previous derivations, until that the components of the ‘‘conventional’’ contribution are written as follows:⁴¹

$$\epsilon_{ij}^C = \delta_{ij} + \delta_{iz} \delta_{jz} e_{zz} + N_{\perp}^{\delta_{iz} + \delta_{jz}} \chi_{ij}^C, \tag{7}$$

where, for instance,

$$\begin{aligned} \chi_{xx}^C &= \frac{1}{z^2} \sum_{\beta} \frac{\omega_{p\beta}^2}{\Omega_*^2} \frac{1}{n_{\beta 0}} \sum_{m=1}^{\infty} \left(\frac{q_{\perp}}{r_{\beta}} \right)^{2(m-1)} \\ &\quad \times \sum_{n=-m}^m n^2 a(|n|, m - |n|) J(n, m, 0; f_{\beta 0}), \\ \chi_{xy}^C &= i \frac{1}{z^2} \sum_{\beta} \frac{\omega_{p\beta}^2}{\Omega_*^2} \frac{1}{n_{\beta 0}} \sum_{m=1}^{\infty} \left(\frac{q_{\perp}}{r_{\beta}} \right)^{2(m-1)} \\ &\quad \times \sum_{n=-m}^m n m a(|n|, m - |n|) J(n, m, 0; f_{\beta 0}), \\ \chi_{yx}^C &= -i \frac{1}{z^2} \sum_{\beta} \frac{\omega_{p\beta}^2}{\Omega_*^2} \frac{1}{n_{\beta 0}} \sum_{m=1}^{\infty} \left(\frac{q_{\perp}}{r_{\beta}} \right)^{2(m-1)} \\ &\quad \times \sum_{n=-m}^m n m a(|n|, m - |n|) J(n, m, 0; f_{\beta 0}), \\ \chi_{yy}^C &= \frac{1}{z^2} \sum_{\beta} \frac{\omega_{p\beta}^2}{\Omega_*^2} \frac{1}{n_{\beta 0}} \sum_{m=1}^{\infty} \left(\frac{q_{\perp}}{r_{\beta}} \right)^{2(m-1)} \\ &\quad \times \sum_{n=-m}^m b(|n|, m - |n|) J(n, m, 0; f_{\beta 0}), \end{aligned} \tag{8}$$

where we have defined the following integral expression:

$$J(n, m, h; f_{\beta 0}) \equiv z \int d^3u \frac{u_{\parallel}^h u_{\perp}^{2(m-1)} u_{\perp} L(f_{\beta 0})}{z - n r_{\beta} - q_{\parallel} u_{\parallel} + i \sum_j \tilde{\nu}_{\beta d}^{j0}}, \tag{9}$$

and where we have utilized the following dimensionless variables

$$\begin{aligned} z &= \frac{\omega}{\Omega_*}, \quad q_{\parallel} = \frac{k_{\parallel} v_*}{\Omega_*}, \quad q_{\perp} = \frac{k_{\perp} v_*}{\Omega_*}, \\ r_{\beta} &= \frac{\Omega_{\beta}}{\Omega_*}, \quad \tilde{\nu}_{\beta d}^{j0}(u) = \frac{\nu_{\beta d}^{j0}(u)}{\Omega_*}. \end{aligned}$$

The differential operator appearing in Eq. (9) is defined as follows:

$$L = \left[(1 - N_{\parallel}^* u_{\parallel}) \frac{\partial}{\partial u_{\perp}} + N_{\parallel}^* u_{\perp} \frac{\partial}{\partial u_{\parallel}} \right],$$

Moreover, we have the following quantities:

$$\begin{aligned} \omega_{p\beta}^2 &= \frac{4\pi n_{\beta 0} q_{\beta}^2}{m_{\beta}}, \quad \Omega_{\beta} = \frac{q_{\beta} B_0}{m_{\beta} c}, \\ a(n, m) &= \left(\frac{1}{2} \right)^{2(|n|+m)} \frac{(-1)^m [2(|n| + m)]!}{[(|n| + m)!]^2 (2|n| + m)! m!}, \\ b(n, m) &= \begin{cases} a(1, m - 2), & \text{for } n = 0 \\ \frac{1}{4} [a(n - 1, m) + a(n + 1, m - 2) \\ - 2 \frac{|n| + m - 1}{|n| + m} a(n, m - 1)], & \text{for } n > 0 \end{cases} \end{aligned}$$

with

$$\frac{1}{(-m)!} = 0, \quad \text{for } m \geq 1,$$

and the explicit form for the equilibrium value of the inelastic collision frequency,

$$\nu_{\beta d}^{j0}(u) = \frac{\pi a_j^2 n_{d0}^j v_*}{u} \left(u^2 + \frac{2Z_{d0}^j e q_\beta}{a_j m_\beta v_*^2} \right) H \left(u^2 + \frac{2Z_{d0}^j e q_\beta}{a_j m_\beta v_*^2} \right). \quad (10)$$

The subscript $\beta = e, i$ identifies electrons and ions, respectively, $q_{d0} = -eZ_{d0}$ is the equilibrium charge of the dust particles, assumed to be negative due to the greater collisional rate of the electrons with the dust particles, compared to the ions, and H denotes the Heaviside function.

The quantities Ω_* and v_* are some characteristic angular frequency and velocity, respectively. For instance, v_* may be the light speed c , or the Alfvén speed v_A , or the ion sound speed c_s , depending on the application for which the formulation is utilized. The integral form given by Eq. (9) depends on the quantity u , which is the normalized momentum, defined as $\mathbf{u} = \mathbf{p}/(m_\alpha v_*)$.

The form of the “conventional” components of the dielectric tensor, as given by Eq. (7), is obtained after expansion of the Bessel functions that appear in components of the dielectric tensor, for magnetized plasmas. The expansion introduces the coefficients $a(n, m)$ and $b(n, m)$, and allows the ε_{ij}^C to be written in such a way that they depend on a double series, on harmonic and Larmor radius contributions. It is seen that the ε_{ij}^C also depend on a small number of integrals, which have to be evaluated depending on the equilibrium distribution function.

The evaluation of the “new” contribution can proceed along similar steps. However, for the present application, we will neglect the “new” contribution, as in previous analysis of the dispersion relation for Alfvén waves.^{34,35,43} The point is that the “new” contributions contain integrals over velocity variables that are similar to those of the “conventional” contributions, but multiplied by the small ratio between the frequency of collisions with dust particles and a characteristic frequency, which is assumed as the ion cyclotron frequency in the case of Alfvén waves. In another example, in the case of electrostatic waves, it has already been shown that the effect of the “new” contribution is negligible, for small population of dust particles.⁴¹

The formulation which has been presented is valid for general forms of the distribution functions of ions and electrons that feature azimuthal symmetry, and constitutes a generalization of previous formulations developed for the case of a single population of dust particles. More complete expressions and more details about the derivation can be found in Refs. 41 and 43.

For the present application, we will consider the case of anisotropic kappa distributions for electrons and ions

$$f_{\beta, \kappa}(\vec{u}) = \frac{n_{\beta 0}}{\pi^{3/2} \kappa_\perp \kappa_\parallel^{1/2} u_\perp^2 u_\parallel} \frac{\Gamma(\kappa_\perp) \Gamma(\kappa_\parallel)}{\Gamma(\kappa_\perp - 1) \Gamma(\kappa_\parallel - 1/2)} \times \left(1 + \frac{u_\parallel^2}{\kappa_\parallel u_\perp^2} \right)^{-\kappa_\parallel} \left(1 + \frac{u_\perp^2}{\kappa_\perp u_\parallel^2} \right)^{-\kappa_\perp}, \quad (11)$$

where

$$u_{\beta\parallel}^2 = \frac{2T_{\beta\parallel}}{m_\beta u_*^2}, \quad u_{\beta\perp}^2 = \frac{2T_{\beta\perp}}{m_\beta u_*^2},$$

and where we have used other dimensionless variables. In order to avoid negative arguments in the Γ functions, the range of values of the κ indexes has to be restricted to $\kappa_\parallel > 0.5$ and $\kappa_\perp > 1.0$. Distribution (11), which is also called “product bi-kappa” distribution, has been utilized in a recent paper presenting a detailed derivation of the components of the dielectric tensor of a dusty plasma and a detailed calculation of the velocity integrals depending on the equilibrium velocity distributions, which appear in these components.⁴³

As it is known, the Maxwellian distribution is the limiting case of kappa distributions when the parameter κ becomes sufficiently large. In Figure 1, we show contour plots for four different forms of the distribution function, vs. u_\parallel and u_\perp , in arbitrary units, for $u_{\beta\parallel} = u_{\beta\perp}$. Figure 1(a) shows the case of a Maxwellian distribution and Figure 1(b) shows distribution (11) for $\kappa_\parallel = \kappa_\perp = 5.0$. It is seen that for equal values of κ_\parallel and κ_\perp , the anisotropic κ distribution is almost symmetrical, with a very slight anisotropy, which can barely be perceived. Panels (c) and (d) of Figure 1 have been obtained for $(\kappa_\parallel = 2.5 \text{ and } \kappa_\perp = 5.0)$ and $(\kappa_\parallel = 5.0 \text{ and } \kappa_\perp = 2.5)$. Despite the difference of a factor 2 between κ_\parallel and κ_\perp , the distribution function still appears to be quite isotropic.

Thermal velocity spreads parallel and perpendicular to the magnetic field can be obtained as second moments of the distribution functions in velocity space. Using spherical coordinates, $u_\parallel = u \cos \theta$ and $u_\perp = u \sin \theta$. The integrals over angular coordinates can be easily performed, and the

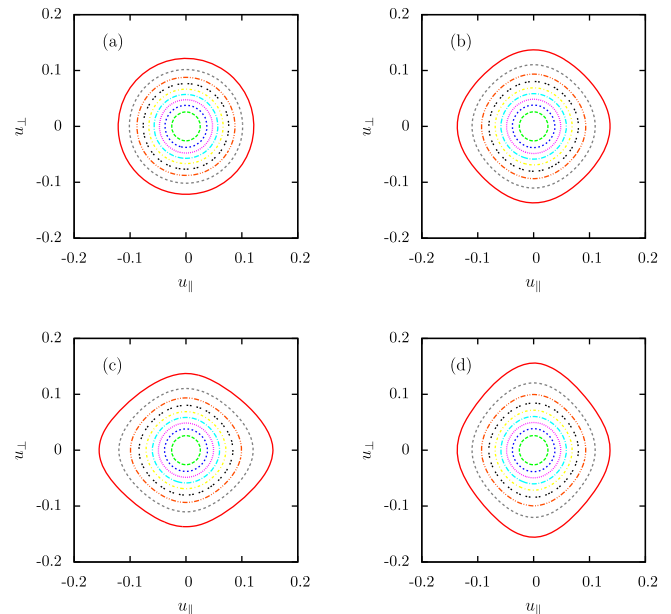


FIG. 1. Contour plots of the electron distribution function vs. u_\parallel and u_\perp , in arbitrary units. (a) Maxwellian distribution function; (b) Anisotropic kappa distribution, with $\kappa_\parallel = \kappa_\perp = 5.0$; (c) Anisotropic kappa distribution, with $\kappa_\parallel = 2.5$ and $\kappa_\perp = 5.0$; and (d) Anisotropic kappa distribution, with $\kappa_\parallel = 5.0$ and $\kappa_\perp = 2.5$.

normalized velocity spreads can be written in terms of the Appell hypergeometrical function of two variables

$$\theta_{\perp}^2 = \frac{4}{3} \frac{2\pi}{\pi^{3/2} \kappa_{\perp} \kappa_{\parallel}^{1/2} u_{\beta\perp}^2 u_{\beta\parallel}} \frac{\Gamma(\kappa_{\perp})\Gamma(\kappa_{\parallel})}{\Gamma(\kappa_{\perp} - 1)\Gamma(\kappa_{\parallel} - 1/2)} \times \int_0^{\infty} du u^4 \left(\frac{\kappa_{\perp} u_{\beta\perp}^2}{\kappa_{\perp} u_{\beta\perp}^2 + u^2} \right)^{\kappa_{\perp}} \times F_1 \left(\frac{1}{2}; \kappa_{\parallel}, \kappa_{\perp}; \frac{5}{2}; -\frac{u^2}{\kappa_{\parallel} u_{\beta\parallel}^2}, \frac{u^2}{\kappa_{\perp} u_{\beta\perp}^2 + u^2} \right), \quad (12)$$

$$\theta_{\parallel}^2 = \frac{2}{3} \frac{2\pi}{\pi^{3/2} \kappa_{\perp} \kappa_{\parallel}^{1/2} u_{\beta\perp}^2 u_{\beta\parallel}} \frac{\Gamma(\kappa_{\perp})\Gamma(\kappa_{\parallel})}{\Gamma(\kappa_{\perp} - 1)\Gamma(\kappa_{\parallel} - 1/2)} \times \int_0^{\infty} du u^4 \left(\frac{\kappa_{\perp} u_{\beta\perp}^2}{\kappa_{\perp} u_{\beta\perp}^2 + u^2} \right)^{\kappa_{\perp}} \times F_1 \left(\frac{3}{2}; \kappa_{\parallel}, \kappa_{\perp}; \frac{5}{2}; -\frac{u^2}{\kappa_{\parallel} u_{\beta\parallel}^2}, \frac{u^2}{\kappa_{\perp} u_{\beta\perp}^2 + u^2} \right). \quad (13)$$

Some additional comments can be made about the thermal dispersion integrals. For these, we utilize the expression written in terms of spherical coordinates, before the integration over u and θ variables,

$$\theta^2 = \frac{2(2\pi)}{\pi^{3/2} \kappa_{\perp} \kappa_{\parallel}^{1/2} u_{\beta\perp}^2 u_{\beta\parallel}} \frac{\Gamma(\kappa_{\perp})\Gamma(\kappa_{\parallel})}{\Gamma(\kappa_{\perp} - 1)\Gamma(\kappa_{\parallel} - 1/2)} \times \int_0^1 d\mu \int_0^{\infty} du u^4 \left(1 + \frac{u^2 \mu^2}{\kappa_{\parallel} u_{\beta\parallel}^2} \right)^{-\kappa_{\parallel}} \left(1 + \frac{u^2 (1 - \mu^2)}{\kappa_{\perp} u_{\beta\perp}^2} \right)^{-\kappa_{\perp}}, \quad (14)$$

where $\mu = \cos \theta$. Of course, θ_{\perp}^2 and θ_{\parallel}^2 can be obtained by inserting μ^2 and $(1 - \mu^2)$ in the integrand, respectively.

Let us analyze the integrand in Eq. (14) in terms of the dependence on u , for $u_{\beta\parallel} = u_{\beta\perp}$, initially considering

$\mu = 0.5$. For $u \rightarrow 0$, the integrand vanishes, and for $u \rightarrow \infty$, the integrand goes as $u^{2(2-\kappa_{\parallel}-\kappa_{\perp})}$. It is seen that it is necessary to have $\kappa_{\parallel} + \kappa_{\perp} > 2$, otherwise the integrand of the thermal dispersion integrals is divergent.

Let us now make further considerations. In the limiting value $\mu = 0$, the integrand of the u integral vanishes for $u \rightarrow 0$ and goes to infinity as $u^{2(2-\kappa_{\perp})}$. The convergence of the integrand depends only on κ_{\perp} , which would have to be larger than 2. That means that, in the region of the integrand where $0 < \mu \ll 0.5$, the integrand converges if $\kappa_{\parallel} + \kappa_{\perp} > 2$, but the meaningful part of the integrand goes up to very large values of u , tending to ∞ for μ approaching 0. Similar reasoning can be made for $\mu = 1$. In the limiting case $\mu = 1$, the integrand would only converge in $\kappa_{\parallel} > 2$. If this condition is not satisfied but $\kappa_{\parallel} + \kappa_{\perp} > 2$, the integrand converges, but the significant part tends to the region $u \rightarrow \infty$, for μ tending to 1. The consequence is that the thermal dispersion, the effective temperature, becomes very different of the Maxwellian case if either κ_{\parallel} or κ_{\perp} becomes smaller than 2, even if the summation $\kappa_{\perp} + \kappa_{\parallel}$ is larger than 2.

These considerations can be illustrated by plots of the integrand of the thermal dispersion integrals. In Figure 2(a), we show the plot obtained considering u^2 multiplying a Maxwellian distribution function, and in Figure 2(b), the case of u^2 multiplying distribution (11) with $\kappa_{\parallel} = \kappa_{\perp} = 5.0$. For these relatively large values of the κ -indexes, despite the fact that the distribution function appeared very similar to the Maxwellian in Figure 1(b), Figure 2(b) shows that the integrand of the thermal dispersion integral is significantly different from the Maxwellian case. Figures 2(c) and 2(d) are similar to Figure 2(b), but with $\kappa_{\parallel} = 2.5$ and $\kappa_{\perp} = 5.0$ in panel (c) and $\kappa_{\parallel} = 5.0$ and $\kappa_{\perp} = 2.5$ in panel (d). Figure 2(c) illustrates that for κ_{\parallel} significantly smaller than κ_{\perp} , the integrand of the thermal dispersion integral can be considerably extended along the parallel direction, and Figure 2(d) shows that for κ_{\perp} significantly smaller than κ_{\parallel} , there is also significant enhancement along perpendicular direction, although less pronounced.

It is also useful to analyze separately the cases of parallel and perpendicular thermal dispersions. In Figure 3, we display the integrand of the thermal integrals, θ_{\parallel}^2 and θ_{\perp}^2 , in arbitrary

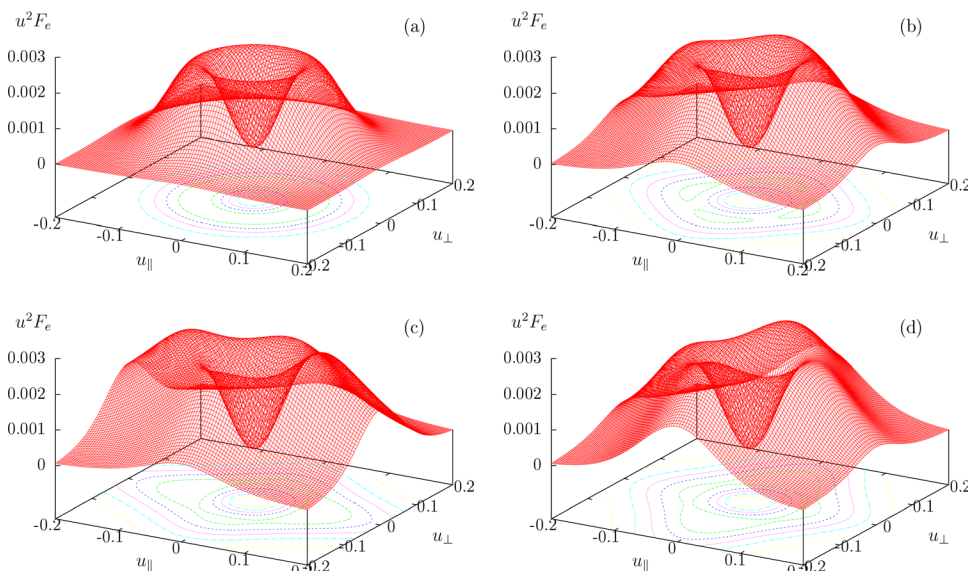


FIG. 2. $u^2 \times$ the electron distribution function vs. u_{\parallel} and u_{\perp} , in arbitrary units. (a) The case of a Maxwellian distribution function; (b) The case of an anisotropic kappa distribution, with $\kappa_{\parallel} = \kappa_{\perp} = 5.0$; (c) The case of an anisotropic kappa distribution, with $\kappa_{\parallel} = 2.5$ and $\kappa_{\perp} = 5.0$; and (d) The case of an anisotropic kappa distribution, with $\kappa_{\parallel} = 5.0$ and $\kappa_{\perp} = 2.5$.

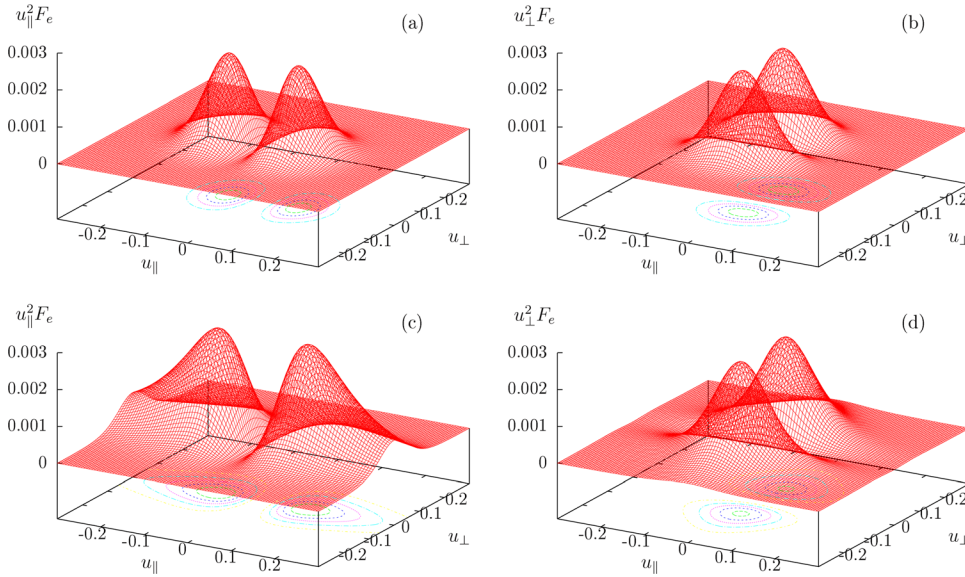


FIG. 3. (a) $u_{\parallel}^2 \times$ the Maxwellian electron distribution function vs. u_{\parallel} and u_{\perp} , in arbitrary units. (b) $u_{\perp}^2 \times$ the Maxwellian electron distribution function vs. u_{\parallel} and u_{\perp} , in arbitrary units. (c) $u_{\parallel}^2 \times$ the anisotropic kappa distribution, with $\kappa_{\parallel} = 2.5$ and $\kappa_{\perp} = 5.0$; and (d) $u_{\perp}^2 \times$ the anisotropic kappa distribution, with $\kappa_{\parallel} = 2.5$ and $\kappa_{\perp} = 5.0$.

units, as function of u_{\parallel} and u_{\perp} , still considering $u_{\beta\parallel} = u_{\beta\perp}$. Figures 3(a) and 3(b), respectively, display the integrands of θ_{\parallel}^2 and θ_{\perp}^2 , for a Maxwellian distribution. Figures 3(c) show respectively the integrands of θ_{\parallel}^2 and θ_{\perp}^2 , considering an anisotropic kappa distribution with $\kappa_{\parallel} = 2.5$ and $\kappa_{\perp} = 5.0$. Panel (d) shows that the integrand of θ_{\perp}^2 is only slightly more extended than the Maxwellian counterpart featured in panel (b), indicating that the perpendicular “temperature” is not significantly different from the temperature in the equilibrium distribution. Panel (c), however, is already well extended toward larger values of u , despite κ_{\parallel} is larger than 2. The significant region of the integrand would extend towards much larger values of u for κ_{\parallel} approaching 2, and extend to infinity if $\kappa_{\parallel} < 2$. The conclusion is that, for κ_{\perp} relatively large, the effective parallel temperature may become very large for κ_{\parallel} approaching the value 2. Similar considerations, about perpendicular effective temperature, could be made in the case of κ_{\perp} smaller than κ_{\parallel} and approaching the value 2.

III. DISPERSION RELATION

Considering waves propagating parallelly to the external magnetic field, the general dispersion relation is obtained from the following determinant:

$$\det \begin{pmatrix} 1 + \chi_{xx}^C - N_{\parallel}^2 & \chi_{xy}^C & 0 \\ \chi_{yx}^C & 1 + \chi_{yy}^C - N_{\parallel}^2 & 0 \\ 0 & 0 & 1 + e_{zz} \end{pmatrix} = 0, \quad (15)$$

where $N_{\parallel} = q_{\parallel}c/v_{*z}$. This dispersion relation factors into two equations, one for electrostatic waves, given by $1 + e_{zz} = 0$, and another for electromagnetic waves, given by 2×2 determinant

$$(1 + \chi_{xx}^C - N_{\parallel}^2)(1 + \chi_{yy}^C - N_{\parallel}^2) - \chi_{xy}^C \chi_{yx}^C = 0, \quad (16)$$

where the χ_{ij}^C are the limiting forms of Eq. (8), for $q_{\perp} \rightarrow 0$,

$$\chi_{xx} = \frac{1}{4z^2} \sum_{\beta} \frac{\omega_{p\beta}^2}{\Omega_{*}^2} \frac{1}{n_{\beta 0}} [J(-1, 1, 0; f_{\beta 0}) + J(1, 1, 0; f_{\beta 0})],$$

$$\chi_{xy} = i \frac{1}{4z^2} \sum_{\beta} \frac{\omega_{p\beta}^2}{\Omega_{*}^2} \frac{1}{n_{\beta 0}} [J(1, 1, 0; f_{\beta 0}) - J(-1, 1, 0; f_{\beta 0})],$$

$$\chi_{yx} = -i \frac{1}{4z^2} \sum_{\beta} \frac{\omega_{p\beta}^2}{\Omega_{*}^2} \frac{1}{n_{\beta 0}} [J(1, 1, 0; f_{\beta 0}) - J(-1, 1, 0; f_{\beta 0})],$$

$$\chi_{yy} = \frac{1}{4z^2} \sum_{\beta} \frac{\omega_{p\beta}^2}{\Omega_{*}^2} \frac{1}{n_{\beta 0}} [J(1, 1, 0; f_{\beta 0}) + J(-1, 1, 0; f_{\beta 0})],$$

where we have used $a(1, 0) = b(1, 0) = 1/4$ and $b(0, 1) = 0$.

It is readily seen that $\chi_{xy}^C = -\chi_{yx}^C$ and that $\chi_{xx}^C = \chi_{yy}^C$, and, therefore, Eq. (16) takes the form

$$(1 + \chi_{xx}^C - N_{\parallel}^2)^2 + (\chi_{xy}^C)^2 = 0. \quad (17)$$

It follows from this equation that the parallel component of refractive index can be expressed as:

$$N_{\parallel}^2 = 1 + \chi_{xx}^C \pm i\chi_{xy}^C \quad (18)$$

or using explicitly the expressions obtained for the χ_{ij}^C ,

$$N_{\parallel}^2 = 1 + \frac{1}{2z^2} \sum_{\beta} \frac{\omega_{p\beta}^2}{\Omega_{*}^2} \frac{1}{n_{\beta 0}} J(s, 1, 0; f_{\beta 0}), \quad (19)$$

where $s = \pm 1$.

For the case of distribution (11), the integral $J(s, 1, 0; f_{\beta 0})$ can be written as follows:

$$\begin{aligned} J(s, 1, 0; f_{\beta 0}) &= 2n_{\beta 0} \frac{\kappa_{\perp}}{\kappa_{\perp} - 2} \\ &\times \left[-\frac{\kappa_{\perp} - 2}{\kappa_{\perp}} + \frac{u_{\beta\perp}^2 \kappa_{\parallel} - 1/2}{u_{\beta\parallel}^2 \kappa_{\parallel}} \right. \\ &\left. + (\zeta_{\beta}^0 - \hat{\zeta}_{\beta}^s) \frac{\kappa_{\perp} - 2}{\kappa_{\perp}} Z_{\kappa_{\parallel}}^0(\hat{\zeta}_{\beta}^s) + \frac{u_{\beta\perp}^2}{u_{\beta\parallel}^2} \hat{\zeta}_{\beta}^s Z_{\kappa_{\parallel}}^1(\hat{\zeta}_{\beta}^s) \right], \end{aligned} \quad (20)$$

where

$$\zeta_\beta^0 = \frac{z}{q_\parallel u_{\beta\parallel}}, \quad \zeta_\beta^n = \frac{z - nr_\beta + i \sum_j \tilde{v}_\beta^j}{q_\parallel u_{\beta\parallel}},$$

$$Z_{\kappa_\parallel}^{(0)}(\zeta) = i \frac{\kappa_\parallel - 1/2}{\kappa_\parallel^{3/2}} \times {}_2F_1 \left[1, 2\kappa_\parallel, \kappa_\parallel + 1; \frac{1}{2} \left(1 + \frac{i\zeta}{\kappa_\parallel^{1/2}} \right) \right],$$

$$\kappa_\parallel > -1/2,$$

$$Z_{\kappa_\parallel}^{(1)}(\zeta) = i \frac{(\kappa_\parallel - 1/2)(\kappa_\parallel + 1/2)}{\kappa_\parallel^{3/2}(\kappa_\parallel + 1)} \times {}_2F_1 \left[1, 2\kappa_\parallel + 2, \kappa_\parallel + 2; \frac{1}{2} \left(1 + \frac{i\zeta}{\kappa_\parallel^{1/2}} \right) \right],$$

$$\kappa_\parallel > -3/2,$$

and ${}_2F_1$ is the Gauss hypergeometric function. Details of the derivation can be obtained in Sec. III of Ref. 43.

Using Eq. (20) into Eq. (19), we get

$$\frac{c^2}{v_*^2} q_\parallel^2 = z^2 + \sum_\beta \frac{\omega_{p\beta}^2}{\Omega_*^2} \left[-1 + \frac{\kappa_\perp}{\kappa_\perp - 2} \frac{\kappa_\parallel - 1/2}{\kappa_\parallel} \frac{u_{\beta\perp}^2}{u_{\beta\parallel}^2} + (\zeta_\beta^0 - \hat{\zeta}_\beta^s) Z_{\kappa_\parallel}^{(0)}(\hat{\zeta}_\beta^s) + \frac{\kappa_\perp}{\kappa_\perp - 2} \frac{u_{\beta\perp}^2}{u_{\beta\parallel}^2} \hat{\zeta}_\beta^s Z_{\kappa_\parallel}^{(1)}(\hat{\zeta}_\beta^s) \right]. \tag{21}$$

By taking the limits $\kappa_\parallel \rightarrow \infty, \kappa_\perp \rightarrow \infty$, and considering the isothermal case $u_{\beta\parallel} = u_{\beta\perp}$, Eq. (21) becomes

$$\frac{c^2}{v_*^2} q_\parallel^2 = z^2 + \sum_\beta \frac{\omega_{p\beta}^2}{\Omega_*^2} \zeta_\beta^0 Z(\hat{\zeta}_\beta^s), \tag{22}$$

which corresponds to the Maxwellian limiting case of Eq. (21).

IV. NUMERICAL ANALYSIS

In the numerical analysis, we will consider electromagnetic waves of low frequency, propagating parallel to the ambient magnetic field. We make the convenient choice, $v_* = v_A, \Omega_* = \Omega_i$. Since distribution (11) was considered, both κ_\perp and κ_\parallel variables are restricted to the intervals^{37,44} $1 < \kappa_\perp < \infty, 1/2 < \kappa_\parallel < \infty$. In addition, closer inspection of the dispersion relation, given by Eq. (21), shows that it is necessary also to impose the condition $\kappa_\perp \neq 2$.

The numerical approach follows that used in Ref. 35, as well as the numerical parameters. Magnetic field, $B_0 = 1.0 \times 10^{-4}$ T, ion density, $n_{i0} = 1.0 \times 10^9$ cm⁻³, $T_{i\parallel} = T_{i\perp} = 1.0 \times 10^4$ K, $T_{e\parallel} = T_{i\parallel}$, and $T_{e\perp} = T_{i\perp}$. For simplicity, we consider only one species of dust particle, with radius, $a = 1.0 \times 10^{-4}$ cm. With the choice of $T_{\beta\perp} = T_{\beta\parallel}$, the anisotropy of the distribution is associated only to the values of κ_\parallel and κ_\perp and to the intrinsically anisotropic character of the bi-kappa distribution.

We start the numerical analysis considering fixed values of κ_\parallel , namely 2.50 and 40.00, and then considered four values of κ_\perp , (2.50, 3.50, 10.0, 40.0). In the sequence, we consider fixed values of κ_\perp , 2.50 and 40.00, and for each of these values, we have evaluated the roots by considering four values of κ_\parallel , (2.50, 3.50, 10.0, 40.0). For all the cases, we consider a single value of the numerical value of the parallel component of the normalized wave vector, $q_\parallel = 0.3$. We present the solutions of the dispersion relation as a function of the parameter ϵ , which varies from 0 to 7×10^{-5} and represents the normalized density of dust particles. In the figures, we consider only the case $s = +1$, since the case $s = -1$ produces equivalent roots. The corresponding roots for the case of Maxwellian distribution are also plotted, for comparison.

In the following, the figures are composed by pairs, side by side, of real and imaginary parts of the normalized frequency z .

A. $\kappa_\parallel = 2.50$

The first case to be considered is the case of $\kappa_\parallel = 2.50$, with κ_\perp between 2.50 and 40.0. In Figure 4, we present four pairs of curves, obtained for $\kappa_\perp = 2.50, 3.50, 10.0$, and 40.0, and also present a pair of curves corresponding to the two modes obtained for the case of isotropic Maxwellian distribution. The curves for the Maxwellian case are presented in black lines. Notice that, even for κ_\perp as large as 40.0, the dispersion curves are still quite far from those in the Maxwellian limit, due to the markedly non-thermal of the distribution along parallel direction, which is associated to $\kappa_\parallel = 2.50$. As it is well known, for small wave number, the dispersion relation for Alfvén waves in a dustless plasma is given by $\omega = kv_A$, where v_A is the Alfvén velocity. For larger wave numbers, the dispersion relation separates into two branches, one known as the *whistler branch* and the other known as the *ion-cyclotron branch*. For $\epsilon \rightarrow 0$, Figure 4(a) denotes with a black dashed line the root corresponding to the forward propagating waves in the whistler branch, and with the black continuous line the solution corresponding to backward propagating waves in the ion-cyclotron branch. In the presence of dust, the real part of the two roots approaches each other. In Figure 4(a), which shows the real part of the normalized frequency, z_r , we notice that there is a crossing of the lines corresponding to the two different roots, for $\epsilon \simeq 6.0 \times 10^{-5}$. On the right-hand panel, one sees that the imaginary part of the two roots is well separated. By comparison between the real and imaginary parts, it is seen that one of the roots is that starting with the dashed line, for small values of ϵ , and continuing with the full line, for ϵ in the upper part of the range considered. This root corresponds to the whistler branch, while the root depicted with the full black line for small values of ϵ and continued with the dashed line corresponds to the branch of the ion-cyclotron waves. There is a coupling between the two modes, at $\epsilon \simeq 6.0 \times 10^{-5}$.³⁵ Figure 4 features in color magenta the curves corresponding to the case of $\kappa_\parallel = 2.50$ and $\kappa_\perp = 40.0$. Both the real and imaginary parts of z are similar in shape to those obtained for the

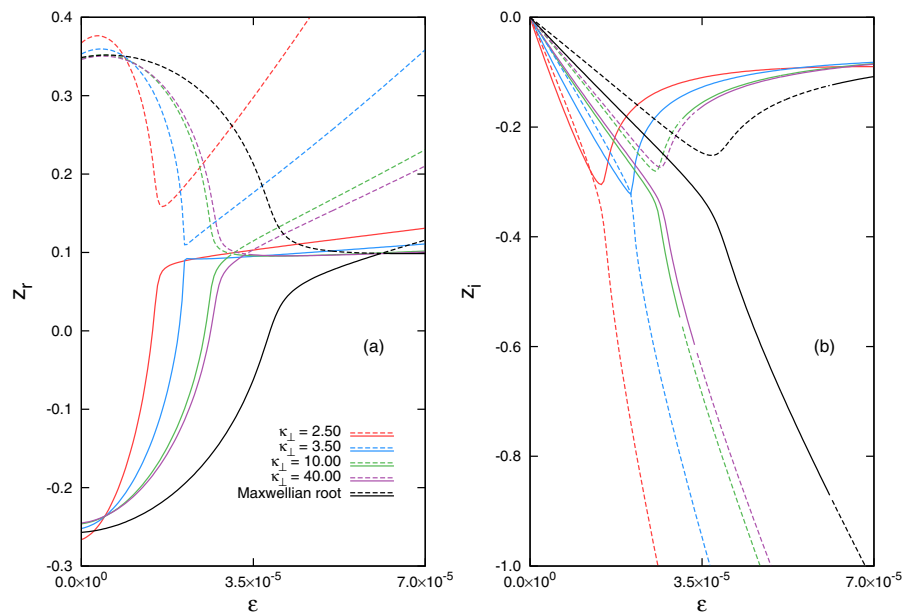


FIG. 4. (a) Real part of the normalized wave frequency, $z_r = \omega_r/\Omega_i$, vs. normalized dust density, $\epsilon = n_d/n_i$, for $\kappa_{||} = 2.50$ and four values of κ_{\perp} , 2.50, 3.50, 10.0, and 40.0. (b) Imaginary part of the normalized wave frequency, $z_i = \omega_i/\Omega_i$, vs. normalized dust density, $\epsilon = n_d/n_i$, for $\kappa_{||} = 2.50$ and four values of κ_{\perp} , 2.50, 3.50, 10.0, and 40.0. Magnetic field $B_0 = 1.0 \times 10^{-4}$ T, ion density $n_{i0} = 1.0 \times 10^9$ cm $^{-3}$, $T_{i||} = T_{i\perp} = 1.0 \times 10^4$ K, $T_{e||} = T_{e\perp}$, and $T_{e\perp} = T_{i\perp}$, only one size of dust particle, $a = 1.0 \times 10^{-4}$ cm.

Maxwellian case, but the point of mode-coupling is moved toward a value of ϵ which is considerably smaller than that of the Maxwellian case, namely $\epsilon \simeq 3.5 \times 10^{-5}$. Another difference is that the magnitude of the damping rates is larger than in the case of the Maxwellian distribution. The case of $\kappa_{||} = 2.50$ and $\kappa_{\perp} = 10.0$ appears in Figure 4 depicted with green lines. It is noticed that the roots of the dispersion relation for $\kappa_{\perp} = 10.0$ are very similar to those of the case with $\kappa_{\perp} = 40.0$, with the mode-coupling point occurring for a value of ϵ only slightly smaller.

On the other hand, Figure 4 also shows the case of $\kappa_{\perp} = 3.50$, depicted with blue lines. Figure 4(a) shows that the two roots come close to each other for $\epsilon \simeq 3.0 \times 10^{-5}$, but the point of mode coupling does not occur. For smaller values of κ_{\perp} , the coupling between the two modes becomes even more distant, as illustrated by the case of $\kappa_{\perp} = 2.50$, shown with red lines in Figures 4(a) and 4(b).

B. $\kappa_{||} = 40.00$

Here, we consider a large value of $\kappa_{||}$, and four values of κ_{\perp} , from small to large, namely $\kappa_{\perp} = 2.50, 3.50, 10.0$, and 40.0. The lines in color magenta and green in Figure 5 represent the cases of $\kappa_{\perp} = 40.0$ and 10.0, respectively. It is seen that the solution of the dispersion relation in these cases is very similar to the solution obtained for Maxwellian distribution, shown by the black lines. The difference is more significant for larger values of ϵ , representing greater dust population, with a displacement of the point of mode coupling toward smaller values of ϵ . Even for the case of $\kappa_{\perp} = 3.50$, depicted with the blue lines, the roots are very similar to the roots of the Maxwellian case, for small ϵ . However, in this case, the point of mode coupling occurs for a content of dust that is less than half of the content required in the Maxwellian case. The case of $\kappa_{\perp} = 2.50$ is shown with red lines in Figure 5. It is seen that the roots corresponding

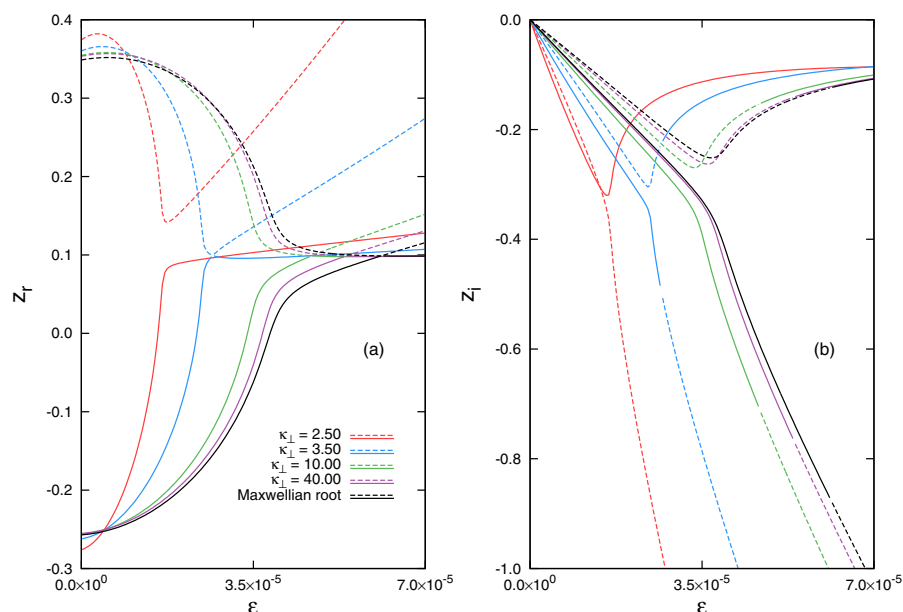


FIG. 5. (a) Real part of the normalized wave frequency, $z_r = \omega_r/\Omega_i$, vs. normalized dust density, $\epsilon = n_d/n_i$, for $\kappa_{||} = 40.0$ and four values of κ_{\perp} , 2.50, 3.50, 10.0, and 40.0. (b) Imaginary part of the normalized wave frequency, $z_i = \omega_i/\Omega_i$, vs. normalized dust density, $\epsilon = n_d/n_i$, for $\kappa_{||} = 40.0$ and four values of κ_{\perp} , 2.50, 3.50, 10.0, and 40.0. Other parameters as in Figure 4.

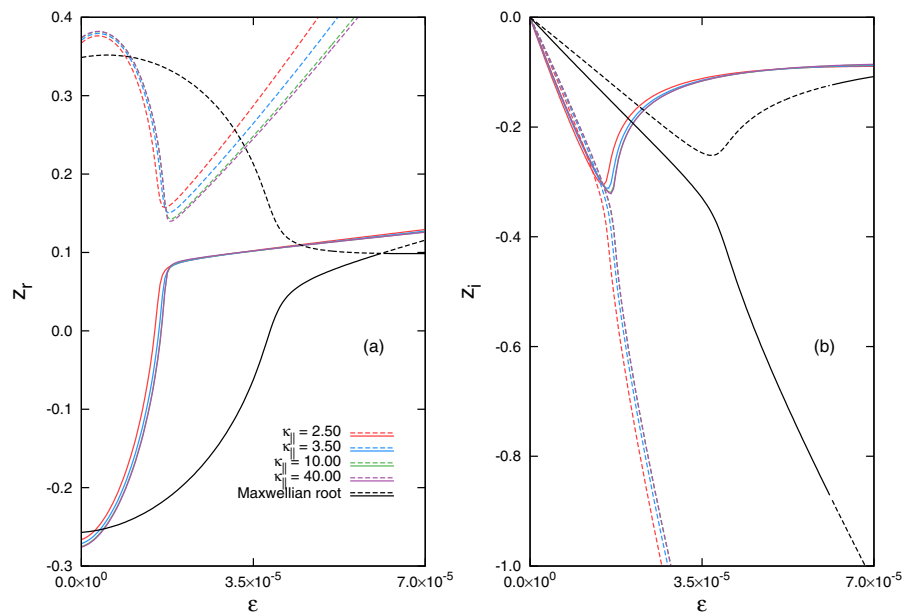


FIG. 6. (a) Real part of the normalized wave frequency, $z_r = \omega_r/\Omega_i$, vs. normalized dust density, $\epsilon = n_d/n_i$, for $\kappa_\perp = 2.50$ and four values of κ_\parallel , 2.50, 3.50, 10.0, and 40.0. (b) Imaginary part of the normalized wave frequency, $z_i = \omega_i/\Omega_i$, vs. normalized dust density, $\epsilon = n_d/n_i$, for $\kappa_\perp = 2.50$, and four values of κ_\parallel , 2.50, 3.50, 10.0, and 40.0. Other parameters as in Figure 4.

to the two branches of the dispersion relation approach to each other in the presence of dust, and then diverge again, without the occurrence of the mode coupling which occurs for Maxwellian plasmas. Despite the fact that the large value of κ_\parallel , 40.0, assures a Maxwellian-like feature to the distribution of velocities along parallel direction, the non-thermal feature associated to small values of κ_\perp produces significant modification of the wave dispersion properties, with the consequent disappearance of the mode coupling, which occurs for in the Maxwellian case, for the parameters considered.

C. $\kappa_\perp = 2.50$

Results obtained in the case of small value of κ_\perp and a range of values of κ_\parallel are shown in Figure 6, with the real part z_r appearing in Figure 6(a) and the imaginary part z_i appearing in Figure 6(b). Differently of the case of small value of κ_\parallel , shown in Figure 4, which displayed marked dependency of the dispersion relation on the value of κ_\perp , Figure 6 shows that the solutions of the dispersion relation for small value of κ_\perp are relatively independent of the value of κ_\parallel . The lines shown in magenta, green, blue, and red, respectively, corresponding to $\kappa_\parallel = 40.0, 10.0, 3.50$, and 2.50, are remarkably close to each other, both in the case of the real part and in the case of the imaginary part. The roots of the dispersion relation are close to the Maxwellian roots for $\epsilon \rightarrow 0$, and depart considerably from the thermal case with the increase of the dust content. The difference regarding the Maxwellian case even for large values of κ_\parallel is associated to the non-thermal feature of the distribution function, which is consequence of the small value of κ_\perp , which is 2.50. It is seen from Figure 6 that the coupling of the two modes does not occur for small value of κ_\perp , for the parameters considered, independently of the value of κ_\parallel . Regarding the imaginary part z_i , Figure 6(b) shows that for the case of small κ_\perp , the damping due to the presence of dust is much more significant than in the Maxwellian case, for small values of ϵ .

D. $\kappa_\perp = 40.00$

Results obtained in the case of large value of κ_\perp and a range of values of κ_\parallel are shown in Figures 7(a) and 7(b). It is readily seen that Figure 7 has a feature markedly different from that seen in Figure 6, obtained for $\kappa_\perp = 2.50$. The solutions obtained for $\kappa_\perp = 40$ and for values of κ_\parallel ranging from the small value $\kappa_\parallel = 2.50$ up to the large value $\kappa_\parallel = 40.0$ are all quite similar to the solutions obtained in the Maxwellian case. The similarity is quite evident from the qualitative point of view, with the quantitative difference that with the decrease of κ_\parallel the point of mode coupling moves toward smaller values of ϵ , that is, the coupling occurs for smaller content of dust, with the increase in the non-thermal features of the parallel distribution. However, it must be remarked that the results show that the mode coupling occurs for the whole range of values of κ_\parallel , in the case of large κ_\perp .

V. FINAL REMARKS

In this paper, we have presented a discussion about numerical results obtained from a dispersion relation for low-frequency electromagnetic propagating along the ambient magnetic field, in a dusty plasma containing a population of dust particles assumed to be spherical and motionless. The dispersion relation was obtained using a kinetic theory, in which we assumed that the interaction between dust particles and plasma particles occur via collisional charging of the dust particles, by inelastic collisions with ions and electrons.

In addition to the presence of the dust, we have assumed that the plasma particles are described by anisotropic κ distributions. Both the presence of dust particles and the non-thermal character of the distribution, described by the κ distributions as well as the presence of anisotropy, are features motivated by observed features in the solar wind.

We have obtained that the dispersion relation for Alfvén waves is significantly affected by the presence of the dust, and significantly affected by the non-thermal features

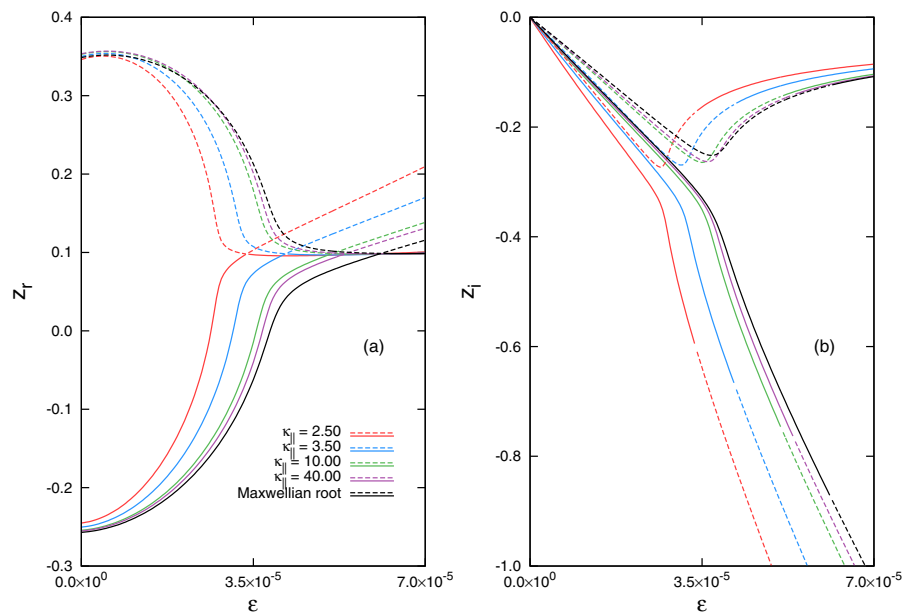


FIG. 7. (a) Real part of the normalized wave frequency, $z_r = \omega_r / \Omega_i$, vs. normalized dust density, $\epsilon = n_d / n_i$, for $\kappa_{\perp} = 40.0$ and four values of κ_{\parallel} , 2.50, 3.50, 10.0, and 40.0. (b) Imaginary part of the normalized wave frequency, $z_i = \omega_i / \Omega_i$, vs. normalized dust density, $\epsilon = n_d / n_i$, for $\kappa_{\perp} = 40.0$ and four values of κ_{\parallel} , 2.50, 3.50, 10.0, and 40.0. Other parameters as in Figure 4.

associated to the anisotropic kappa distributions. For small value of κ_{\parallel} , mode coupling occurs between waves in the whistler branch and waves in the ion-cyclotron branch, for sufficiently large dust population, if κ_{\perp} is above a limiting value, but ceases to occur for small values of κ_{\perp} . Even for large values of κ_{\parallel} , exemplified in the present paper by $\kappa_{\parallel} = 40.0$, the results obtained are similar, in the sense that mode coupling continues to occur at sufficiently large dust population, for most of the range of values of κ_{\perp} . Only for $\kappa_{\perp} \lesssim 3.0$, the dispersion relation departs sufficiently from the Maxwellian case, such that the mode coupling does not occur, regardless the dust population.

On the other hand, we have shown that for small value of κ_{\perp} , exemplified by $\kappa_{\perp} = 2.50$, the mode coupling does not occur, for the whole range of values of κ_{\parallel} . For $\kappa_{\perp} = 40.0$, example of a large value, the situation is reversed: mode coupling occurs for the whole range of κ_{\parallel} . The qualitative conclusion which can be drawn is that the non-thermal feature along the perpendicular direction seems to dominate the dispersion relation, regarding the proximity with the results expected for thermal plasmas. Even for relatively moderated values of κ_{\perp} , for which the distribution functions of plasma particles is approximately Maxwellian along the perpendicular direction, the dispersion properties of Alfvén waves do not depart very much from the behavior of thermal plasmas. On the other hand, even for very large values of κ_{\parallel} , corresponding to a completely Maxwellian shape along the parallel direction, the dispersive properties of Alfvén waves in a dusty plasma only approach those of Maxwellian plasmas for sufficiently high value of κ_{\perp} . For small κ_{\perp} , the results of the dispersion relation for Alfvén waves are significantly different from those of thermal plasmas, independently of the value of κ_{\parallel} . These findings correspond to those obtained in the case of anisotropic Maxwellian distributions, for which the mode coupling between circularly polarized and whistler branches was observed to remain when parallel temperature is larger than perpendicular temperature, and disappear when perpendicu-

lar temperature becomes sufficiently larger than parallel temperature.³⁶

The objective of the paper has been to investigate the dependency of the dispersion relation on the parameters κ_{\parallel} and κ_{\perp} , and on the presence of the dust. For this analysis, the temperature parameter T has been considered isotropic, with the anisotropy in the distribution function associated entirely to the parameters κ_{\parallel} and κ_{\perp} . Despite the highly anisotropic situations considered in the analysis, we have not obtained unstable solutions in the dispersion relation, for the parameters considered. We intend to continue the investigation by considering different parameters, in order to determine how instabilities like the firehose instability and the ion-cyclotron instability are affected by the simultaneous presence of dust and non-thermal kappa distributions. The results of the forthcoming investigation on the instabilities shall be submitted for publication in the near future.

¹E. Marsch, Living Rev. Solar Phys. **3**, 1 (2006); available at <http://www.livingreview.org/lrsp-2006-1>.

²R. Schwenn, *Space Sci. Rev.* **124**, 51 (2006).

³N. Altobelli, Ph.D. dissertation University of Heidelberg, Heidelberg, Germany, 2004, see <http://d-nb.info/972033629>.

⁴I. Mann, H. Kimura, D. A. Biesecker, B. T. Tsurutani, E. Grün, E. R. B. McKibben, J. C. Liou, R. M. MacQueen, T. Mukai, M. Guhathakurta, and P. Lamy, *Space Sci. Rev.* **110**, 269 (2004).

⁵I. Mann, *Adv. Space Res.* **41**, 160 (2008).

⁶H. Kruger, M. Landgraf, N. Altobelli, and E. Grun, *Space Sci. Rev.* **130**, 401 (2007).

⁷E. Grün, H. A. Zook, H. Fechting, and R. H. Giese, *Icarus* **62**, 244 (1985).

⁸H. Ishimoto and I. Mann, *Planet. Space Sci.* **47**, 225 (1998).

⁹N. Meyer-Vernet, M. Maksimovic, A. Czechowski, I. Mann, I. Zouganelis, K. Goetz, M. L. Kaiser, O. C. St. Cyr, J. L. Bougeret, and S. D. Bale, *Solar Phys.* **256**, 463 (2009).

¹⁰E. Marsch *et al.*, *J. Geophys. Res.* **87**, 52 (1982).

¹¹E. Marsch, L. Zhao, and C.-Y. Tu, *Ann. Geophys.* **24**, 2057 (2006).

¹²L. Matteini, S. Landi, P. Hellinger, F. Pantellini, M. Maksimovic, M. Velli, B. E. Goldstein, and E. Marsch, *Geophys. Res. Lett.* **34**, L20105, doi:10.1029/2007GL030920 (2007).

¹³P. Hellinger, P. Trávníček, J. C. Kasper, and A. J. Lazarus, *Geophys. Res. Lett.* **33**, L09101, doi:10.1029/2006GL025925 (2006).

- ¹⁴M. D. Montgomery, S. J. Bame, and A. J. Hundhaus, *J. Geophys. Res.* **73**, 4999, doi:10.1029/JA073i015p04999 (1968).
- ¹⁵W. C. Feldman, J. R. Asbridge, J. S. Bame, M. D. Montgomery, and S. P. Gary, *J. Geophys. Res.* **90**, 4181, doi:10.1029/JA080i031p04181 (1975).
- ¹⁶R. P. Lin, D. W. Potter, D. A. Gurnett, and F. L. Scarf, *Astrophys. J.* **251**, 364 (1981).
- ¹⁷R. P. Lin, W. K. Levedahl, W. Lotko, D. A. Gurnett, and F. L. Scarf, *Astrophys. J.* **308**, 954 (1986).
- ¹⁸W. Pilipp, H. Miggenrieder, M. Montgomery, K.-H. Mühlhäuser, H. Rosenbauer, and R. Schwenn, *J. Geophys. Res.* **91**, 1075, doi:10.1029/JA092iA02p01075 (1987).
- ¹⁹W. Pilipp, H. Miggenrieder, M. Montgomery, K.-H. Mühlhäuser, H. Rosenbauer, and R. Schwenn, *J. Geophys. Res.* **92**, 1093, doi:10.1029/JA092iA02p01093 (1987).
- ²⁰R. J. Fitzenreiter, W. Ogilvie, D. J. Chornay, and J. Keller, *Geophys. Res. Lett.* **25**, 249, doi:10.1029/97GL03703 (1998).
- ²¹V. Pierrard, M. Maksimovic, and J. Lemaire, *Astron. Astrophys.* **277**, 195 (2001).
- ²²C. Pagel, N. U. Crooker, D. E. Larson, S. W. Kahler, and M. J. Owens, *J. Geophys. Res.* **110**, A01103, doi:10.1029/2004JA010767 (2005).
- ²³C. Pagel, S. P. Gary, C. A. de Koning, and R. M. Skoug, *J. Geophys. Res.* **112**, A04103, doi:10.1029/2006JA011967 (2007).
- ²⁴V. M. Vasyliunas, *J. Geophys. Res.* **73**, 2839, doi:10.1029/JA073i009p02839 (1968).
- ²⁵M. Maksimovic, V. Pierrard, and J. F. Lemaire, *Astron. Astrophys.* **324**, 725 (1997).
- ²⁶M. Maksimovic, I. Zouganelis, J.-Y. Chaufray, K. Issautier, E. E. Scime, J. E. Littleton, E. Marsch, D. J. McComas, C. Salem, R. P. Lin, and H. Elliot, *J. Geophys. Res.* **110**, A09104, doi:10.1029/2005JA011119 (2005).
- ²⁷S. Stverak, M. Maksimovic, P. M. Travnicek, E. Marsch, A. N. Fazakerley, and E. E. Scime, *J. Geophys. Res.* **114**, A05104, doi:10.1029/2008JA013883 (2009).
- ²⁸M. P. Leubner, *Phys. Plasmas* **11**, 1308 (2004).
- ²⁹P. H. Yoon, *Phys. Plasmas* **19**, 052301 (2012).
- ³⁰F. Huang, Y. Chen, G. Shi, Z. Hu, H. Peng, J. Zheng, and M. Y. Yu, *Phys. Plasmas* **16**, 042107 (2009).
- ³¹M. Lazar, R. Schlickeiser, and S. Poedts, *Phys. Plasmas* **17**, 062112 (2010).
- ³²M. Lazar, S. Poedts, and R. Schlickeiser, *Mon. Not. R. Astron. Soc.* **410**, 663 (2011).
- ³³G. I. Sukhinin and A. V. Fedoseev, *Plasma Phys. Rep.* **33**, 1023 (2007).
- ³⁴M. C. de Juli, R. S. Schneider, L. F. Ziebell, and V. Jatenco-Pereira, *Phys. Plasmas* **12**, 052109 (2005).
- ³⁵L. F. Ziebell, M. C. de Juli, R. S. Schneider, and V. Jatenco-Pereira, *Phys. Plasmas* **12**, 082102 (2005).
- ³⁶M. C. de Juli, R. S. Schneider, L. F. Ziebell, and R. Gaelzer, *Phys. Plasmas* **14**, 022104 (2007).
- ³⁷R. Gaelzer, M. C. de Juli, and L. F. Ziebell, *J. Geophys. Res.* **115**, A09109, doi:10.1029/2009JA015217 (2010).
- ³⁸L. J. Spitzer, *Physical Processes in the Interstellar Medium* (Wiley, New York, 1978).
- ³⁹V. N. Tsytovich and O. Havnes, *Commun. Plasma Phys. Controlled Fusion* **15**, 267 (1993).
- ⁴⁰M. C. de Juli and R. S. Schneider, *J. Plasma Phys.* **60**, 243 (1998).
- ⁴¹L. F. Ziebell, R. S. Schneider, M. C. de Juli, and R. Gaelzer, *Braz. J. Phys.* **38**, 297 (2008).
- ⁴²M. C. de Juli and R. S. Schneider, *J. Plasma Phys.* **64**, 57 (2000).
- ⁴³R. A. Galvão, L. F. Ziebell, R. Gaelzer, and M. C. de Juli, *Braz. J. Phys.* **41**, 258 (2011).
- ⁴⁴M. P. Leubner, *Astrophys. Space Sci.* **282**, 573 (2002).